Geophysical Research Letters

RESEARCH LETTER
10.1029/2023GL104916

# Detecting Signatures of Convective Storm Events in GNSS-SNR: Two Case Studies From Summer 2021 in Switzerland

**Matthias Aichinger-Rosenberger[1], Martin Aregger[2,3], Jerome Kopp[2,3], and Benedikt Soja[1]**

[1]Institute of Geodesy and Photogrammetry, ETH Zurich, Zurich, Switzerland, [2]Institute of Geography, University of Bern, Bern, Switzerland, [3]Oeschger Center for Climate Change Research, University of Bern, Bern, Switzerland

**Key Points:**

- GNSS
- Severe storm detection
- Signal-to-Noise ratio

**Supporting Information:**

Supporting Information may be found in the online version of this article.

**Correspondence to:**

M. Aichinger-Rosenberger, maichinger@ethz.ch

**Citation:**

Aichinger-Rosenberger, M., Aregger, M., Kopp, J., & Soja, B. (2023). Detecting signatures of convective storm events in GNSS-SNR: Two case studies from summer 2021 in Switzerland. *Geophysical Research Letters*, *50*, e2023GL104916. https://doi.org/10.1029/2023GL104916

Received 9 JUN 2023
Accepted 19 OCT 2023

**Author Contributions:**

**Conceptualization:** Matthias Aichinger-Rosenberger
**Data curation:** Matthias Aichinger-Rosenberger, Martin Aregger, Jerome Kopp, Benedikt Soja
**Formal analysis:** Matthias Aichinger-Rosenberger, Martin Aregger, Jerome Kopp, Benedikt Soja
**Investigation:** Matthias Aichinger-Rosenberger, Martin Aregger, Jerome Kopp
**Methodology:** Matthias Aichinger-Rosenberger, Martin Aregger, Jerome Kopp
**Resources:** Matthias Aichinger-Rosenberger, Martin Aregger, Jerome Kopp, Benedikt Soja
**Software:** Matthias Aichinger-Rosenberger, Martin Aregger, Jerome Kopp
**Supervision:** Benedikt Soja
**Validation:** Matthias Aichinger-Rosenberger, Martin Aregger, Jerome Kopp



**Abstract** Global Navigation Satellite Systems (GNSS) are not only a state-of-the-art sensor for positioning and navigation applications but also a valuable tool for remote sensing. Through the usage of L-band carrier frequencies, GNSS acts as an all-weather-operation system, offering substantial benefits compared to optical systems. Nevertheless, severe weather can still have an impact on the strength of signals received at a ground station, as we show in this study. We investigate GNSS Signal-to-Noise Ratio (SNR) observations during two severe convective storm events over the city of Zurich, Switzerland. We make use of a GNSS-SNR-based algorithm originally developed for the detection of hail particles from volcanic eruptions. Results indicate that, although GNSS observations are considered to be fairly insensitive to the presence of hydrometeors, convective storm events are visible in SNR observations. SNR levels of affected satellites show a significant drop during event periods, which are determined by weather radar observations.

**Plain Language Summary** Over the last two decades, observations from Global Navigation Satellite Systems (GNSS) have proven to be a useful data source for meteorology. Typically, signal delays introduced by the presence of water vapor along the signal path are utilized for analyzing and predicting the atmospheric moisture field, and subsequently, precipitation. However, other GNSS observations types can also be influenced by severe thunder- and hailstorms, which are high-impact weather events. In this study, we show that is the case for the Signal-to-Noise Ratio (SNR) of GNSS signals. We investigate two large thunderstorm events which took place over the city of Zurich. These events are visible as significant degradation in SNR data of GNSS satellites. By analyzing radar images we are able to show that the time period of SNR degradation closely corresponds to the period of strongest precipitation intensity observed by radar. Although more detailed investigations have to be carried out in the future, these initial findings indicate the potential of GNSS-SNR data for observation of severe weather events and strengthen the status of GNSS as a valuable tool for meteorological applications.

## 1. Introduction

Extreme weather events, such as severe thunderstorms and associated natural hazards, represent a significant risk to human life and property through lightning, heavy precipitation, hail and strong winds. These phenomena are very localized in space and can develop within timescales ranging from tens of minutes to a few hours, making them difficult to forecast precisely using numerical weather prediction (NWP) models. As most climate projections indicate an increasing frequency of such events in most regions (Rädler et al., 2019; Ridder et al., 2022), accurate forecasts and observational methods as well as the development of early warning and resilience systems become increasingly important.

Existing satellite-based detection of severe, hail-producing convection in literature is based on proxy methods which link characteristics such as microwave brightness temperatures (e.g., Ferraro et al., 2015; Laviola et al., 2020) and overshooting cloud tops (e.g., Khlopenkov et al., 2021; Murillo, 2022; Punge et al., 2023) to storm severity and hail probability. In recent years, also machine learning-based convection detection approaches have become more commonplace (e.g., Cintineo et al., 2020; McGovern et al., 2023; Zha et al., 2021). Direct detection methods, however, are rare and mostly rely on specific instrumentation, which is often specifically developed and installed for hail observation in rather small local networks. In this study, we investigate the possibility of using existing infrastructure in form of Global Navigation Satellite Systems (GNSS) stations for such detection tasks.

**Visualization:** Matthias Aichinger-Rosenberger, Martin Aregger, Jerome Kopp
**Writing – original draft:** Matthias Aichinger-Rosenberger
**Writing – review & editing:** Martin Aregger, Jerome Kopp, Benedikt Soja

Over the last two decades, GNSS have been established as a state-of-the-art observation system for navigation and monitoring purposes. In atmospheric sciences, troposphere products from GNSS are recognized as valuable data sources for NWP and climate monitoring. The presence of atmospheric water vapor affects signal propagation by causing a delay in GNSS signals, which can be determined alongside the receiver coordinates and clock error. This technique, commonly referred to as GNSS Meteorology (Bevis et al., 1992), has been used extensively for data assimilation systems at almost all major NWP centers worldwide and its benefits have been shown by a large number of studies (see Guerova et al. (2016) or Jones et al. (2020) for a good overview). Over the last years, an increasing number of authors have focused on signatures of severe weather events, such as extreme precipitation (e.g., Arief & Heki, 2020; Wilgan et al., 2023).

In contrast to GNSS Meteorology, which requires a comprehensive GNSS processing approach to determine tropospheric signal delays, other techniques have been established that make use of raw GNSS observations. One example is GNSS Reflectometry (GNSS-R), a technique that aims to infer information about the surface from which a reflected signal travels to the receiver. This way, quantities such as soil moisture (K. Larson et al., 2008) or snow depth (K. Larson et al., 2009) can be retrieved. Furthermore, space-borne GNSS-R retrievals are able to sense precipitation over the ocean by quantifying the rain attenuation impact on GNSS-R wind speed products (Asgarimehr et al., 2018, 2019). For ground-based GNSS-R, the basic observation type is the Signal-to-Noise Ratio (SNR) of GNSS signals (GNSS-SNR). In GNSS processing, SNR often only represents an indication of data quality and the level of multipath interference. Besides this, it is still rarely used in GNSS data analysis. In addition to the impact of surface properties on GNSS-SNR, there are also processes which can affect the SNR of direct signals. One example is volcanic eruptions, which have been studied using GNSS observations by a number of authors over the last decades (e.g., Grapenthin et al., 2022; Lee et al., 2015; Shimada et al., 1990). Most of these studies used GNSS observations to monitor ground deformation near erupting volcanoes, but not to detect effects of the eruption above ground, for example, the evolution of the plume. Modeling of volcanic plumes was first shown by Houlié et al. (2005a) for the eruption of Miyakejima volcano (Japan) and Mount St.Helens (Houlié et al., 2005b) and this approach was developed further by Grapenthin et al. (2013). Most recently, Cegla et al. (2022) investigated the 2014 Sakurajima Eruption, by a comparison of Zenith Total Delays (ZTDs) from GNSS and ray-tracing methods.

All of those studies treated the effects of the plume on signal propagation as an unmodeled atmospheric error, originating from the presence of a large amount of sand and ash particles. This idea is reasonable, since sand and ash particles affect signal propagation in a similar way as gaseous atmospheric constituents, although the magnitude of this effect is smaller. This was shown by Solheim et al. (1999) in a theoretical investigation carried out over two decades ago. They also found that under standard atmospheric conditions, GNSS measurements experience no significant impact from hydrometeors (small amounts of water or ice particles) present along the signal path. However, they also note that this might change for severe weather events, where both the amount and size of hydrometeors are much more substantial. As for volcanic particles, the effect of hydrometeors on GNSS products during severe weather conditions was primarily studied using troposphere products, such as ZTD or Slant Total Delays (STDs). Studies such as Brenot et al. (2006), Douša et al. (2016), or Hordyniec et al. (2018) found significant effects under extreme weather conditions, accounting for a mismodeling of, for example, ZTD of up to cm-level. However, one major disadvantage of investigating hydrometeors as a tropospheric mismodeling is the fact that comprehensive GNSS processing is necessary to derive all products to be analyzed. In order to avoid this, K. M. Larson (2013) introduced a new method for plume detection that is solely based on SNR observations. The study showed the strengths and limitations of the method by presenting results from the 2008 and 2009 eruptions of the Okmok and Mt. Redoubt volcanoes. Plume detections based on GNSS-SNR observations were found to be consistent with independently collected seismic and radar data of the eruptions. In a later study on the 2011 eruption of Grímsvötn Volcano in Iceland, Grapenthin et al. (2018) applied a method that combined SNR and phase residuals to detect volcanic hail.

Our study applies a similar SNR-based detection algorithm as shown in K. M. Larson (2013) on data collected during two severe convective storm events, which affected the city of Zurich in Switzerland in early summer 2021. Using observations from a nearby GNSS station, we show how these storms affect GNSS-SNR and thus allow for the detection of such events. To our knowledge, this study represents the first investigation showing the signature, and subsequently detection, of convective storm events in GNSS-SNR data.

## 2. Data and Methods

### 2.1. GNSS-SNR

SNR is a raw observation type which is typically recorded by all GNSS receivers and serves as a measure of received signal strength. GNSS-SNR levels depend on both satellite elevation and the actual carrier frequency on which observations are recorded. They increase with satellite elevation, peaking at levels between 50 and 60 dB-Hz for satellites observed near the zenith direction (90°). For this study, we utilize SNR observations solely from the Global Positioning System (GPS). The GPS constellation currently consists of 31 satellites, orbiting at an altitude of approximately 20,200 km, where each GPS satellite makes two complete orbits each sidereal day. Due to this repeatability, satellites cover the same elevation ranges (and therefore comparable SNR levels) for approximately the same time periods on consecutive days. We will make use of this fact in our analysis and the formulation of the detection algorithm introduced in Section 2.4. Following K. M. Larson (2013), we use solely GPS L2C SNR data (in the following termed S2) in this study because of its smaller amount of high-frequency noise at higher elevations compared to L1.

For our case studies we utilize SNR observations from ETHZ GNSS station collected at a data rate of 30 s, available in Receiver Independent Exchange Format (RINEX) 2.11 (Gurtner & Estey, 2007). The station is located in the city of Zurich at the ETH Campus Hoenggerberg and belongs to the Automated GNSS Network of Switzerland (AGNES), operated by the Federal Office of Topography (swisstopo).

### 2.2. Radar

As a state-of-the-art observing technique for precipitation, weather radar images are the first choice to accurately determine the thunderstorm event time at the respective GNSS sites. Therefore, we make use of operational radar products, stemming from the Swiss weather radar network (Rad4Alp). The network consists of five polarimetric C-band radars at altitudes ranging from 928 to 2,937 m above sea level, operated by MeteoSwiss (Germann et al., 2022). The radars are arranged in a configuration which provides overlapping coverage, ensuring good visibility in the Alps. Here, we use a two-dimensional Cartesian maximum reflectivity composite with a spatial resolution of 1 km × 1 km which is produced every 5 min and spans an area of 640 × 710 km$^2$. For the composite, the polar horizontal reflectivity data from each of the five radars is interpolated into a three-dimensional Cartesian grid on which a column maximum is applied to reduce it to a two-dimensional data set (Germann et al., 2009; Waldvogel et al., 1979). To identify individual convective cells and their movements, the reflectivity-based Thunderstorm Radar Tracking (TRT) algorithm is used (Hering et al., 2004). The TRT algorithm identifies individual convective cells within a precipitation system using an adaptive reflectivity thresholding scheme on radar images. A convective cell is defined as a contiguous area of radar pixels of at least 16 km$^2$. With a reflectivity that exceeds 36 dBZ, and at least one pixel needs to attain a reflectivity of 42 dBZ (Raupach et al., 2021).

### 2.3. Hail Crowdsourced Reports

Alongside heavy precipitation, severe convective storms also produce hail. While radar-based hail algorithms exist to estimate the probability of hail on the ground (POH, Waldvogel et al., 1979) and the maximum expected severe hailstone size (MESHS, Foote et al., 2005), they are proxy-based and not surface observations. Therefore, we use the crowdsourcing function of the MeteoSwiss app to assess the presence of hail on the ground. The function allows users to report the hail size category, time and location using their smartphone. The reports are previously submitted to plausibility filters to reduce the number of false alarms (Barras et al., 2019).

### 2.4. Detection Algorithm

As mentioned in the introduction, this study makes use of a largely similar plume-detection algorithm as proposed in K. M. Larson (2013). The exact algorithm applied in this study consists of the following steps:

1. Extract GPS-S2 time series from RINEX observation files using the rnx2snr module of the GNSS-IR software gnssrefl (Roesler & Larson, 2018).
2. Filter out all data with elevation angles <20°, which is more likely to be affected by multipath effects

3. Determine useable satellites: Only satellites providing continuous observations during the event time ±1 hr are used.
4. For each utilized satellite:

(a) Shift the obtained SNR time series by 4 min/day (with respect to the event day) to account for the repetition time of GPS satellite geometry (23 hr 56 min)
(b) Average time series for 10 prior non-event days to build up the background model (i.e., average SNR evolution for the respective elevation range)
(c) Obtain SNR residuals for the event day by subtracting the background model from the actual SNR observations
(d) Calculate the mean and standard deviation of SNR residuals ($\sigma_{res}$) from all ten non-event days.
(e) Set the residual mean $\pm 2.5 \cdot \sigma_{res}$ as the nominal level to be used for event detection.

A visual overview of the algorithm, in the form of a flowchart, can be found in Supporting Information S1. In order to test its performance, results of the algorithm for two severe convective storm events are shown in the following sections.

## 3. Convective Storm Case Studies

The month of July 2021 was characterized by a persistent flow bringing moist and unstable air over Switzerland. Thunderstorms occurred regularly with heavy rainfall, hail and strong wind gusts that caused a fair amount of damage (Kopp et al., 2023; MeteoSwiss, 2021a). In the following, we give a short description of two case studies (CS) carried out for thunderstorm events which affected the city of Zurich in early summer 2021, and present results for the application of the detection algorithm outlined in Section 2.4.

### 3.1. CS1: 28.06.2021

On 28.06.2021, several supercell storms originated in Western Switzerland around 14:00 UTC and then moved along the northern flank of the Swiss Alps following southwest to northeast tracks. Some of these supercells merged and evolved in an intense mesoscale convective system which produced the second largest hail event in Switzerland since 2002 (MeteoSwiss, 2021b), and hailstones of up to 9 cm diameter in central Switzerland, southwest of Zurich (Kopp et al., 2023). This mesoscale convective system approached the city of Zurich and the ETHZ GNSS station from the southwest around 16:40 UTC (Figure 1). Extended areas with maximum radar reflectivity (MAXRE) values of up to 60 dBZ were registered (Figure 1a) as well as the largest daily number of hail crowdsourced reports (Figure 1b).

For CS1, the detection algorithm was applied on observations of satellites G4, G17, and G19, which were selected based on the criteria outlined in Section 2.4. Results are presented in Figure 2. The left panel (a) of the figure shows the respective time series of GPS-SNR observations from the event day as well as 2 days prior and after the event day. The right panel (b) shows the results of the detection algorithm with colored points representing SNR residuals for the same days as shown on the left side. During this period, all three satellites show degraded SNR levels compared to the background model, with the largest degradation corresponding to the largest reflectivity values over the station. The same pattern is also captured by the SNR residuals. Although the number of impacted observations is limited (1–3) for each satellite, their degradation level is significant (2–3 db-Hz), capturing a clear impact of the thunderstorm for the event day. In terms of detection performance, the algorithm does reasonably well, although some detections on non-event days are visible for G17 and G19. There are also a few event detections ahead of the actual event time for satellites G4 and G19. Nevertheless, the largest degradations occur exactly during the period of most intense precipitation, giving a strong indication of the storm's impact on SNR levels.

### 3.2. CS2: 12.-13.07.2021

The second storm case investigated in this study took place during the night of 12–13.07.2021, when a supercell thunderstorm crossed Switzerland from France, ahead of an active cold front coming from the west. The storm was particularly intense when it approached the city of Zurich and the ETHZ station from the southwest on 12.07.2021, around 23:40 UTC, with MAXRE values of up to 50 dBZ (Figure 3a). The southwest to northeast movement is clearly visible on the successive MAXRE scans of Figure 3a, with peak reflectivity values lasting for about 20 min over the ETHZ station, until approximately 00:00 UTC. The storm also brought hail as shown

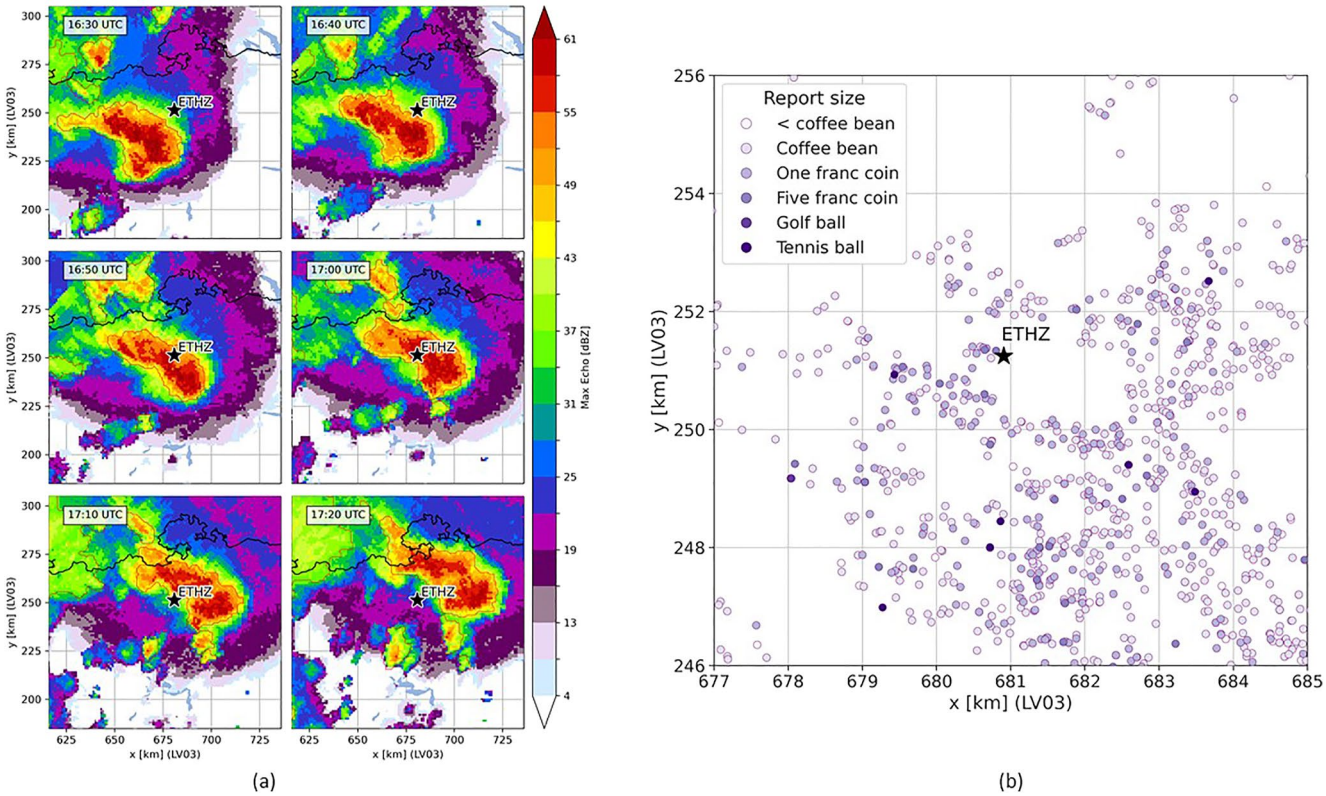


**Figure 1.** Radar and crowdsourced hail observations for CS1, 28.06.2021: (a): Images of MAXRE (dBZ) for the region surrounding the ETH Zurich station. Shown are images in 10 min intervals. (b): Hail observations for the region surrounding the ETH Zurich station: location of crowdsourced reports (purple dots, largest sizes are darker), location of the ETHZ GNSS station (black star).

by the multiple crowdsourced reports sent by the population (Figure 3b). Similar to CS1, the left panel (a) of Figure 4 shows the observed SNR time series of CS2 for satellites G05, G13, and G14, continuously observed during the period of interest (23:00–00:00 UTC). Results show a similar pattern as observed for CS1, that is, a clear degradation in SNR level for all satellites during the period of most intense precipitation (23:40–00:00 UTC) over the ETHZ station. Apart from event time, the observed values agree well with the background model and the noise level is similar throughout the 5 days shown. This further strengthens the evidence of a distinctive thunderstorm impact on the SNR level, with similar characteristics to CS1. The SNR residuals, shown on the right panel (b) of Figure 4, indicate an even stronger impact of this thunderstorm event on SNR at ETHZ. Some false detections prior and after the event, as well as on other days are again visible, but to a much lesser extent than in CS1. In comparison to CS1, the residual levels are slightly lower (mostly 1–2 db-Hz) but the number of observations affected by the storm is much higher. For instance, satellites G13 and G14 show a much larger amount of detected events for the event period than any satellite analyzed for CS1. While only one event was detected for G5, several residuals are close to the detection level, still indicating sustained degradation compared to average SNR levels.

## 4. Discussion and Conclusions

We presented an initial investigation showing the influence of severe convective storms on GNSS-SNR data by discussing two case studies affecting the ETHZ GNSS station on 28.06.2021 and 12.-13.07.2021. Furthermore, we introduced a simple statistical algorithm to detect these events in GNSS-SNR timeseries. Both cases were accompanied by heavy precipitation and hail, as reported by radar images and crowdsourced hail observations. Our results show a clear SNR degradation during the exact event time at ETHZ, which has been determined from the radar images. Although the number of affected observations is quite small, most of these observations show a significant degradation (~2 dB-Hz) compared to average values. These results confirmed both the impact of

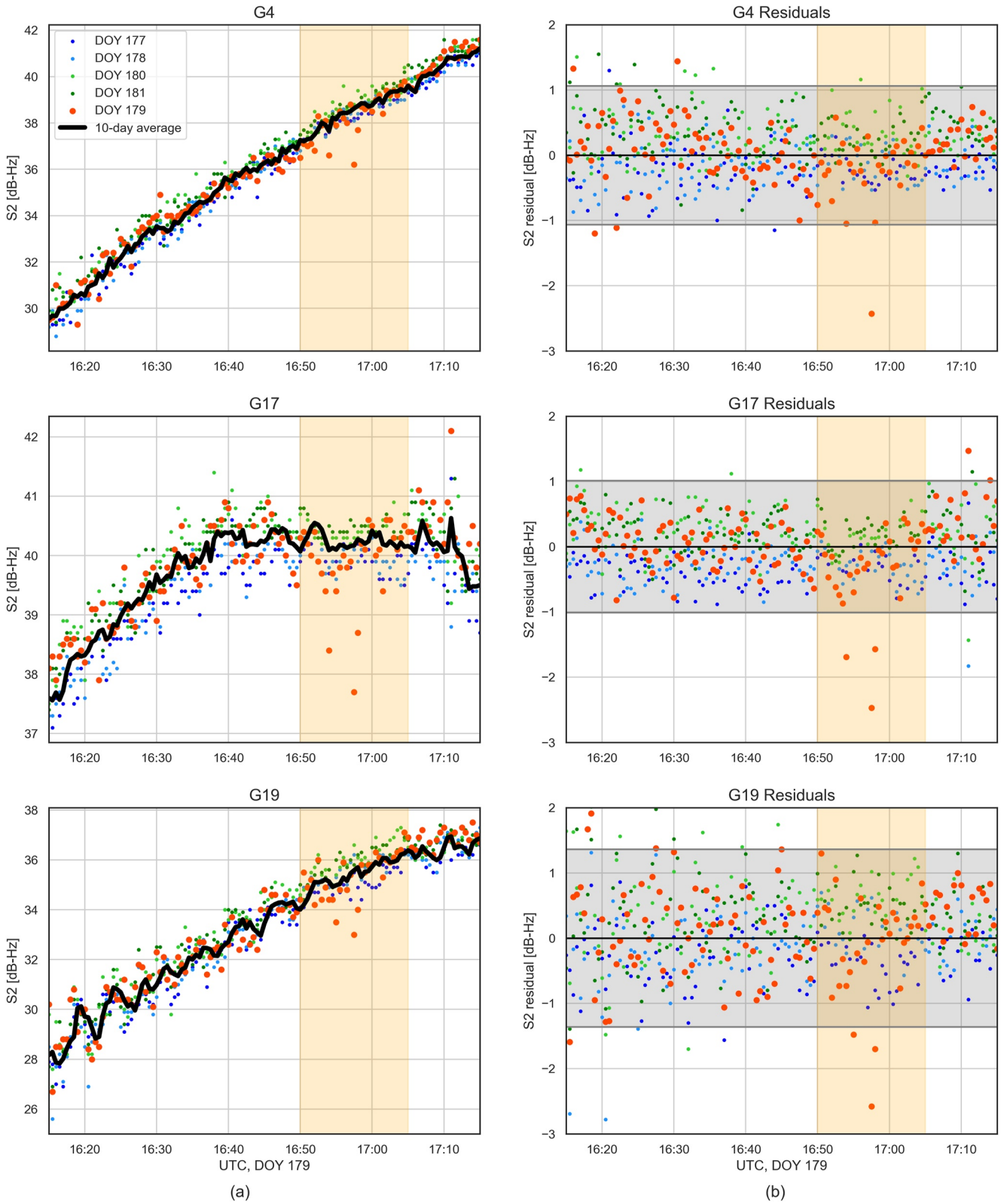


**Figure 2.** (a): SNR observations of satellites G4, G17, and G19 at ETHZ for CS1. Shown are observations from the event day (red, DOY 179), 2 days prior (blue colors, DOY 177/178) and 2 days after (green colors, DOY 180/181). In addition, an average over the last 10 days prior to the event is shown as the black solid line. (b): SNR residuals with respect to the 10-days average for the respective satellite. The nominal detection level is shown as the horizontal gray area. The exact event period determined by radar is color-coded in orange.

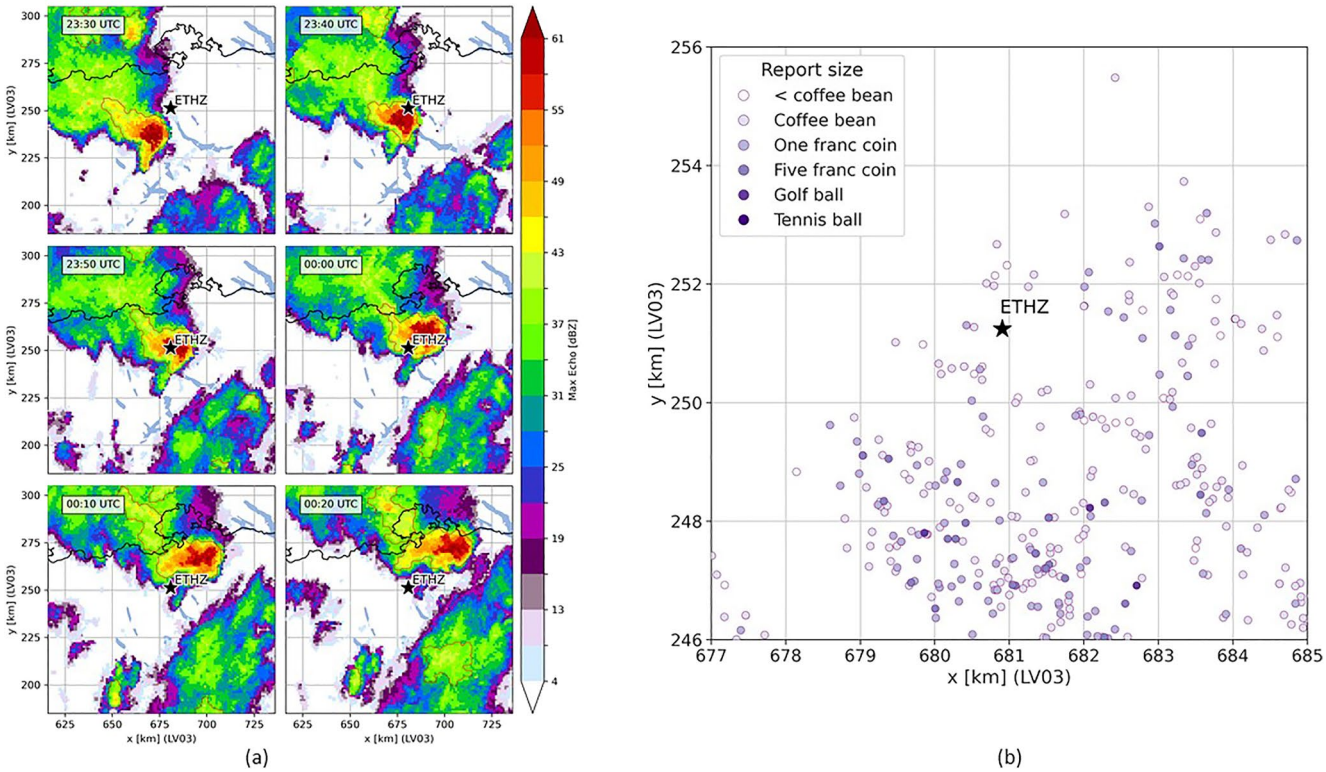


**Figure 3.** Same as Figure 1 but for CS2, 12-13.07.2021: (a): Images of MAXRE (dBZ) for the region surrounding the ETH Zurich stations. Shown are images in 5 min intervals. (b): Hail observations for the region surrounding the ETH Zurich stations on 12-13.07.2021: location of crowdsourced reports (purple dots, largest sizes are darker), location of the ETHZ GNSS station (black star).

severe convective storm events on GNSS-SNR observations and the capability of the proposed algorithm for detecting such events.

For CS1, only 1–3 SNR observations per satellite were impacted, but these observations showed a significant degradation of 2–3 dB-Hz. This degradation was observed at the exact time of maximum storm intensity over the ETHZ station, which gives a clear indication of the storm's impact on the observed SNR levels. In comparison to CS1, the SNR degradation observed for CS2 is of a slightly weaker magnitude but more persistent over time, resulting in a much larger number of observations (about 10–20) being affected. This might indicate that the storm system was more stationary for CS2, but radar images suggest that the duration of maximum storm intensity was about 20 min for both cases. For both cases, some false detections ahead of the actual event time also suggested a possible earlier impact of the approaching storm systems on specific satellites. However, most of the used satellite tracks crossed the storm track only right around event time, which makes an earlier impact unlikely.

The utilized detection algorithm is a very simple statistical approach, which allows for an easy implementation and interpretation of the results. The original algorithm of K. M. Larson (2013), initially developed for the detection of volcanic plumes, was only slightly modified for this study. Our version uses a 10-days average of SNR observations as a background model to calculate SNR residuals and a $2.5 \cdot \sigma_{res}$ detection interval. These parameter settings for the detection algorithm are chosen in order to balance false and missed detection for the investigated events, but should be fine-tuned in future studies. Further results investigating the influence of different settings for the presented events can be found in the additional material of this study.

In general, GNSS-SNR might be used as an additional proxy for detecting storm activity, in the form of individual point observations. The advantages of the proposed detection approach can be summarized as the following:

- High temporal (up to 1 Hz) and spatial coverage (5–10 km in dense networks).
- Practically no additional costs for existing stations and only small costs for establishing new sites.
- Very simple and computationally efficient detection algorithm, allowing for real-time implementation.

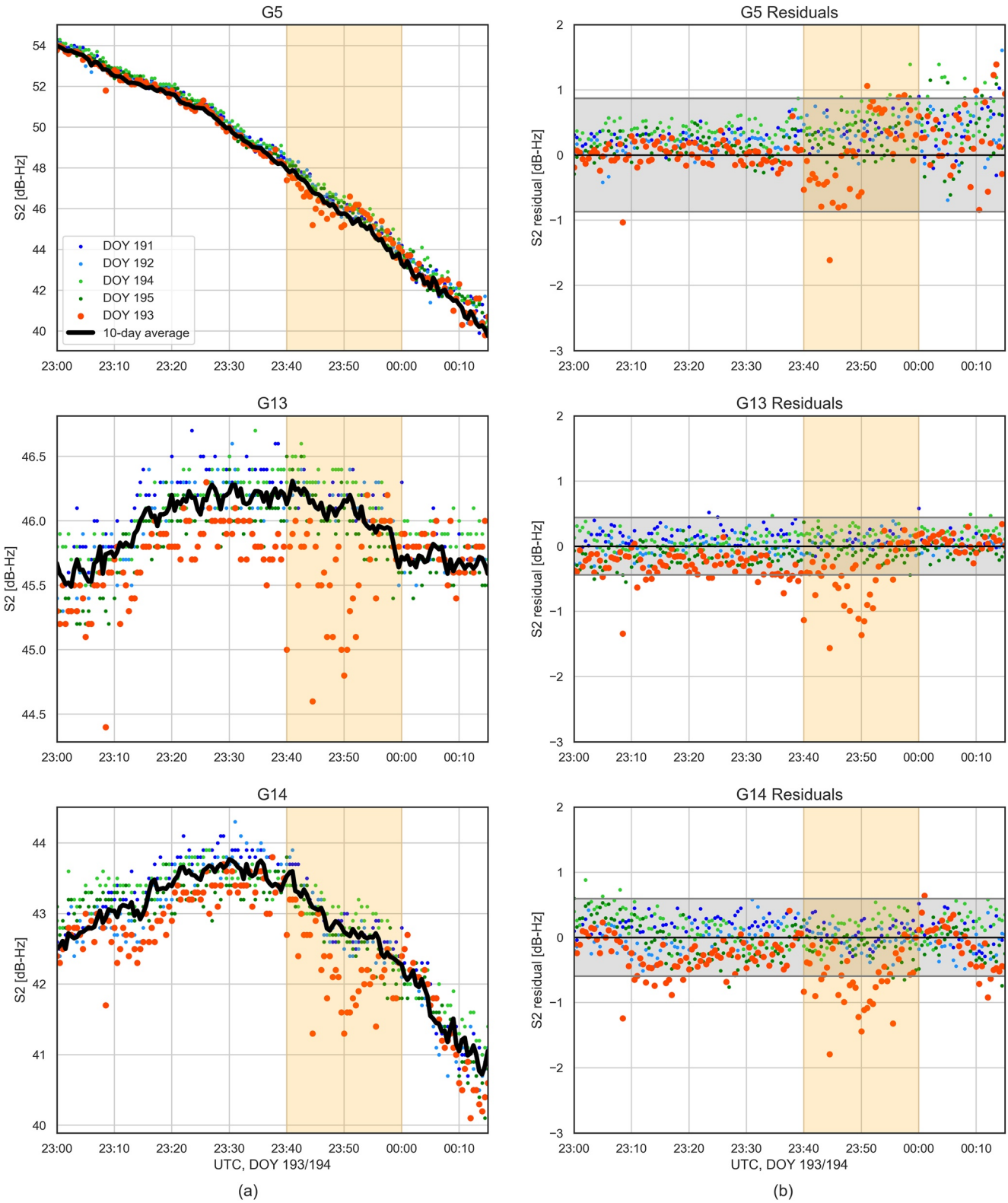


**Figure 4.** (a): SNR observations of satellites G05, G13, and G14 from ETHZ station for time period 12.07.2021 23:00–00:00 UTC. Shown are observations from the event day (red, DOY 193), 2 days prior (blue colors, DOY 191/192) and 2 days after (green colors, DOY 194/195). In addition, an average over the last 10 days prior to the event is shown as the black solid line. (b): SNR residuals with respect to the 10-days average for the respective satellite. The nominal detection level is shown as the horizontal gray area. The exact event period determined by radar is color-coded in orange.

Beside these advantages, our approach also has a number of limitations:

- The sensitivity of GNSS-SNR data is limited (L-band), implying that only severe storms could be detected. This also implies that the storm must travel directly over the GNSS station, in order to produce significant SNR degradation. Results from other stations indicating these limitations can be found in the additional material to this study.
- GNSS-SNR represents an integral value along the ray path. Therefore, the horizontal resolution is restricted to the satellite tracks.
- Precise (sub-integer level) SNR observations are required, which is limiting the choice of GNSS receivers.

At this stage, we can neither quantify the contribution of each hydrometeor type (rain vs. hail), nor the influence of the size of the hydrometeors on the magnitude of the degradation. Furthermore, the contribution of other factors (such as lightning activity) to the SNR degradation is still unclear and thus should be investigated by future studies. Future improvements of the presented approach could come from the usage of multi-GNSS and higher-rate observations (e.g., 1 Hz). In this study, we solely used GPS observations, but in recent years, the evolution of multi-GNSS (with the new GNSS systems Galileo and BeiDou) has broadened the GNSS signal spectrum significantly. Nowadays a variety of signals on different carrier frequencies are available, which could also be used for approaches like the one presented in this study. An extension to other GNSS is relatively straightforward and planned to be implemented for future investigations. This extension will increase the number of available observations by a factor of two to three and therefore strengthen confidence in the presented approach. Moreover, using 1 Hz observations would increase the amount of data used in this study by a factor of 30. Although already existing GNSS stations might not all record multi-GNSS data at these high frequencies, such considerations should be kept in mind when designing new infrastructure. Furthermore, more sophisticated data mining and machine-learning algorithms might be explored, as their capability to reveal weather phenomena in GNSS products, to which observations should not be directly sensitive, has for example, been demonstrated for downslope wind storms (Aichinger-Rosenberger et al., 2022). Thus, such algorithms might also be capable of separating the signatures of different hydrometeor types (rain and hail) in GNSS data. However, this separation denotes a highly complex task, which most likely will not be possible to achieve using SNR data solely. Therefore, the combination of SNR observations with additional GNSS products also impacted by atmospheric conditions, such as tropospheric signal delays and phase residuals, could be explored. Such approaches will hopefully lead to an improved understanding and identification of all factors accounting for the observed SNR degradation. These factors might include the total amount of water along the ray path (substantial for supercell storms), the ratio of gaseous/liquid/solid particles found in clouds or even lightning events. Measuring the properties of hailstorms is a difficult task due to their rarity and small spatial extent. Hence, being able to use existing and future networks of GNSS stations to detect hailstorms could be very useful. Further investigations comparing storms that produced hail with others that did not could help discriminate a hail signature on GNSS signals.

## Data Availability Statement

The GNSS-SNR data sets used in this study are available at Aichinger-Rosenberger (2023).

**Acknowledgments**
We thank MeteoSwiss for providing the radar and crowdsourced data and Swisstopo for providing the GNSS data. M.A. acknowledges support from the Swiss Science Foundation project no. CRSII5_201792 J.K. acknowledges support from the Swiss insurance company La Mobilière.

## References

Aichinger-Rosenberger, M. (2023). GNSS-SNR dataset summer 2021 [Dataset]. ETH Zurich. https://doi.org/10.3929/ethz-b-000636333

Aichinger-Rosenberger, M., Brockmann, E., Crocetti, L., Soja, B., & Moeller, G. (2022). Machine learning-based prediction of alpine foehn events using GNSS troposphere products: First results for Altdorf, Switzerland. *Atmospheric Measurement Techniques*, *15*(19), 5821–5839. https://doi.org/10.5194/amt-15-5821-2022

Arief, S., & Heki, K. (2020). GNSS meteorology for disastrous rainfalls in 2017–2019 summer in SW Japan: A new approach utilizing atmospheric delay gradients. *Frontiers in Earth Science*, *8*. https://doi.org/10.3389/feart.2020.00182

Asgarimehr, M., Wickert, J., & Reich, S. (2019). Evaluating impact of rain attenuation on space-borne GNSS reflectometry wind speeds. *Remote Sensing*, *11*(9), 1048. https://doi.org/10.3390/rs11091048

Asgarimehr, M., Zavorotny, V., Wickert, J., & Reich, S. (2018). Can GNSS reflectometry detect precipitation over oceans? *Geophysical Research Letters*, *45*(22), 12585–12592. https://doi.org/10.1029/2018GL079708

Barras, H., Hering, A., Martynov, A., Noti, P.-A., Germann, U., & Martius, O. (2019). Experiences with > 50,000 crowdsourced hail reports in Switzerland. *Bulletin of the American Meteorological Society*, *100*(8), 1429–1440. https://doi.org/10.1175/BAMS-D-18-0090.1

Bevis, M., Businger, S., Herring, T. A., Anthes, R. A., & Ware, R. H. (1992). GPS meteorology: Remote sensing of atmospheric water vapor using the global positioning system. *Geophysical Magazine*, *34*(D14), 359–425. https://doi.org/10.1029/92jd01517

Brenot, H., Ducrocq, V., Walpersdorf, A., Champollion, C., & Caumont, O. (2006). GPS zenith delay sensitivity evaluated from high-resolution numerical weather prediction simulations of the 8–9 September 2002 flash flood over southeastern France. *Journal of Geophysical Research*, *111*(D15), D15105. https://doi.org/10.1029/2004jd005726

Cegla, A., Rohm, W., Lasota, E., & Biondi, R. (2022). Detecting volcanic plume signatures on GNSS signal, based on the 2014 Sakurajima eruption. *Advances in Space Research*, *69*(1), 292–307. https://doi.org/10.1016/j.asr.2021.08.034

Cintineo, J. L., Pavolonis, M. J., Sieglaff, J. M., Wimmers, A., Brunner, J., & Bellon, W. (2020). A deep-learning model for automated detection of intense midlatitude convection using geostationary satellite images. *Weather and Forecasting*, *35*(6), 2567–2588. https://doi.org/10.1175/WAF-D-20-0028.1

Douša, J., Dick, G., Kačmařík, M., Brožková, R., Zus, F., Brenot, H., et al. (2016). Benchmark campaign and case study episode in central Europe for development and assessment of advanced GNSS tropospheric models and products. *Atmospheric Measurement Techniques*, *9*(7), 2989–3008. https://doi.org/10.5194/amt-9-2989-2016

Ferraro, R., Beauchamp, J., Cecil, D., & Heymsfield, G. (2015). A prototype hail detection algorithm and hail climatology developed with the advanced microwave sounding unit (AMSU). *Atmospheric Research*, *163*, 24–35. https://doi.org/10.1016/j.atmosres.2014.08.010

Foote, G. B., Krauss, T. W., & Makitov, V. (2005). Hail metrics using conventional radar. In *85th AMS annual meeting, American meteorological society* (pp. 2791–2796). Combined Preprints.

Germann, U., Berenguer, M., Sempere-Torres, D., & Zappa, M. (2009). REAL—Ensemble radar precipitation estimation for hydrology in a mountainous region. *Quarterly Journal of the Royal Meteorological Society*, *135*(639), 445–456. https://doi.org/10.1002/qj.375

Germann, U., Boscacci, M., Clementi, L., Gabella, M., Hering, A., Sartori, M., et al. (2022). Weather radar in complex orography. *Remote Sensing*, *14*(3), 503. https://doi.org/10.3390/rs14030503

Grapenthin, R., Freymueller, J. T., & Kaufman, A. M. (2013). Geodetic observations during the 2009 eruption of Redoubt Volcano, Alaska. *Journal of Volcanology and Geothermal Research*, *259*, 115–132. (The 2009 Eruption of Redoubt Volcano, Alaska). https://doi.org/10.1016/j.jvolgeores.2012.04.021

Grapenthin, R., Hreinsdóttir, S., & Van Eaton, A. R. (2018). Volcanic hail detected with GPS: The 2011 eruption of Grímsvötn Volcano, Iceland. *Geophysical Research Letters*, *45*(22), 12236–12243. https://doi.org/10.1029/2018GL080317

Grapenthin, R., Kyle, P., Aster, R. C., Angarita, M., Wilson, T., & Chaput, J. (2022). Deformation at the open-vent Erebus volcano, Antarctica, from more than 20 years of GNSS observations. *Journal of Volcanology and Geothermal Research*, *432*, 107703. https://doi.org/10.1016/j.jvolgeores.2022.107703

Guerova, G., Jones, J., Dousa, J., Dick, G., Haan, S., Pottiaux, E., et al. (2016). Review of the state-of-the-art and future prospects of the ground-based GNSS meteorology in Europe. *Atmospheric Measurement Techniques Discussions*, *9*(11), 5385–5406. https://doi.org/10.5194/amt-9-5385-2016

Gurtner, W., & Estey, L. (2007). *RINEX: The receiver independent exchange format version 2.11*. Astronomical Institute, University of Bern.

Hering, A. M., Morel, C., Galli, G., Senesi, S., Ambrosetti, P., & Boscacci, M. (2004). Nowcasting thunderstorms in the Alpine region using a radar based adaptive thresholding scheme. In *Proceedings of ERAD conference 2004* (pp. 206–211). Retrieved from https://www.copernicus.org/erad/2004/online/ERAD04_P_206.pdf

Hordyniec, P., Kapłon, J., Rohm, W., & Kryza, M. (2018). Residuals of tropospheric delays from GNSS data and ray-tracing as a potential indicator of rain and clouds. *Remote Sensing*, *10*(12), 1917. https://doi.org/10.3390/rs10121917

Houlié, N., Briole, P., Nercessian, A., & Murakami, M. (2005a). Sounding the plume of the 18 august 2000 eruption of Miyakejima volcano (Japan) using GPS. *Geophysical Research Letters*, *32*(5), L05302. https://doi.org/10.1029/2004GL021728

Houlié, N., Briole, P., Nercessian, A., & Murakami, M. (2005b). Volcanic plume above Mount st. Helens detected with GPS. *Eos, Transactions American Geophysical Union*, *86*(30), 277–281. https://doi.org/10.1029/2005EO300001

Jones, J., Guerova, G., Dousa, J., Dick, G., Haan, S., Pottiaux, E., et al. (2020). Advanced GNSS tropospheric products for monitoring severe weather events and climate. In *chap. General Background*. Springer.

Khlopenkov, K. V., Bedka, K. M., Cooney, J. W., & Itterly, K. (2021). Recent advances in detection of overshooting cloud tops from longwave infrared satellite imagery. *Journal of Geophysical Research: Atmospheres*, *126*(14), e2020JD034359. https://doi.org/10.1029/2020JD034359

Kopp, J., Schröer, K., Schwierz, C., Hering, A., Germann, U., & Martius, O. (2023). The summer 2021 Switzerland hailstorms: Weather situation, major impacts and unique observational data. *Weather*, *78*(7), 184–191. https://doi.org/10.1002/wea.4306

Larson, K., Gutmann, E., Zavorotny, V., Braun, J., Williams, M., & Nievinski, F. (2009). Can we measure snow depth with GPS receivers? *Geophysical Research Letters*, *36*(17), L17502. https://doi.org/10.1029/2009GL039430

Larson, K., Small, E., Gutmann, E., Bilich, A., Axelrad, P., & Braun, J. (2008). Using GPS multipath to measure soil moisture fluctuations: Initial results. *GPS Solutions*, *12*(3), 173–177. https://doi.org/10.1007/s10291-007-0076-6

Larson, K. M. (2013). A new way to detect volcanic plumes. *Geophysical Research Letters*, *40*(11), 2657–2660. https://doi.org/10.1002/grl.50556

Laviola, S., Levizzani, V., Ferraro, R. R., & Beauchamp, J. (2020). Hailstorm detection by satellite microwave radiometers. *Remote Sensing*, *12*(4), 621. https://doi.org/10.3390/rs12040621

Lee, S.-W., Yun, S.-H., Kim, D. H., Lee, D., Lee, Y. J., & Schutz, B. E. (2015). Real-time volcano monitoring using GNSS single-frequency receivers. *Journal of Geophysical Research: Solid Earth*, *120*(12), 8551–8569. https://doi.org/10.1002/2014JB011648

McGovern, A., Chase, R. J., Flora, M., Gagne, D. J., Lagerquist, R., Potvin, C. K., et al. (2023). A review of machine learning for convective weather. *Artificial Intelligence for the Earth Systems*, *2*(3). https://doi.org/10.1175/AIES-D-22-0077.1

MeteoSwiss (2021a). Bulletin climatologique juillet 2021. Retrieved from https://www.meteosuisse.admin.ch/services-et-publications/publications/rapports-et-bulletins/2021/bulletin-climatologique-juillet-2021.html

MeteoSwiss (2021b). Bulletin climatologique juin 2021. Retrieved from https://www.meteosuisse.admin.ch/services-et-publications/publications/rapports-et-bulletins/2021/bulletin-climatologique-juin-2021.html

Murillo, E. (2022). Overshooting convection in the contiguous United States: Severe hail occurrence, storm top characteristics, and stratospheric hydration.

Punge, H. J., Bedka, K. M., Kunz, M., Bang, S. D., & Itterly, K. F. (2023). Characteristics of hail hazard in South Africa based on satellite detection of convective storms. *Natural Hazards and Earth System Sciences*, *23*(4), 1549–1576. https://doi.org/10.5194/nhess-23-1549-2023

Rädler, A., Groenemeijer, P., Faust, E., Sausen, R., & Púčik, T. (2019). Frequency of severe thunderstorms across Europe expected to increase in the 21st century due to rising instability. *Npj Climate and Atmospheric Science*, *2*, 1–5. https://doi.org/10.1038/s41612-019-0083-7

Raupach, T. H., Martynov, A., Nisi, L., Hering, A., Barton, Y., & Martius, O. (2021). Object-based analysis of simulated thunderstorms in Switzerland: Application and validation of automated thunderstorm tracking with simulation data. *Geoscientific Model Development*, *14*(10), 6495–6514. https://doi.org/10.5194/gmd-14-6495-2021

Ridder, N., Ukkola, A., Pitman, A., & Perkins-Kirkpatrick, S. (2022). Increased occurrence of high impact compound events under climate change. *Npj Climate and Atmospheric Science*, *5*(1), 3. https://doi.org/10.1038/s41612-021-00224-4

Roesler, C., & Larson, K. (2018). Software tools for GNSS interferometric reflectometry (GNSS-IR). *GPS Solutions*, *22*(3), 80. https://doi.org/10.1007/s10291-018-0744-8

Shimada, S., Fujinawa, Y., Sekiguchi, S., Ohmi, S., Eguchi, T., & Okada, Y. (1990). Detection of a volcanic fracture opening in Japan using Global Positioning System measurements. *Nature*, *343*(6259), 631–633. https://doi.org/10.1038/343631a0

Solheim, F. S., Vivekanandan, J., Ware, R. H., & Rocken, C. (1999). Propagation delays induced in GPS signals by dry air, water vapor, hydrometeors, and other particulates. *Journal of Geophysical Research*, *104*(D8), 9663–9670. https://doi.org/10.1029/1999JD900095

Waldvogel, A., Federer, B., & Grimm, P. (1979). Criteria for the detection of hail cells. *Journal of Applied Meteorology and Climatology*, *18*(12), 1521–1525. https://doi.org/10.1175/1520-0450(1979)018⟨1521:CFTDOH⟩2.0.CO;2

Wilgan, K., Dick, G., Zus, F., & Wickert, J. (2023). Tropospheric parameters from multi-GNSS and numerical weather models: Case study of severe precipitation and flooding in Germany in July 2021. *GPS Solutions*, *27*(1), 49. https://doi.org/10.1007/s10291-022-01379-0

Zha, S., Jin, W., He, C., Chen, Z., Si, G., & Jin, Z. (2021). Detecting of overshooting cloud tops via Himawari-8 imagery using dual channel multiscale deep network. *IEEE Journal of Selected Topics in Applied Earth Observations and Remote Sensing*, *14*, 1654–1664. https://doi.org/10.1109/JSTARS.2020.3044618